Simple model for plasmon enhanced fluorescence correlation spectroscopy

Lutz Langguth* and A. Femius Koenderink

Center for Nanophotonics, FOM Institute AMOLF, Science Park 104, 1098 XG Amsterdam, The Netherlands

**L.Langguth@amolf.nl*

Abstract: Metallic nano-antennas provide strong field confinement and intensity enhancement in hotspots and thus can ultimately enhance fluorescence detection and provide ultra small detection volumes. In solution-based fluorescence measurements, the diffraction limited focus driving the nano-antenna can outshine the fluorescence originating from the hotspot and thus render the benefits of the hotspot negligible. We introduce a model to calculate the effect of a nano-antenna, or any other object creating a nontrivial intensity distribution, for fluorescence fluctuation measurements. Approximating the local field enhancement of the nano-antenna by a 3D Gaussian profile, we show which hotspot sizes and intensities are the most beneficial for an FCS measurement and compare it to realistic antenna parameters from literature.

OCIS codes: (170.2520) Fluorescence microscopy; (310.6628) Subwavelength structures, nanostructures; (350.4238) Nanophotonics and photonic crystals.

References and links

1. J. N. Anker, W. P. Hall, O. Lyandres, N. C. Shah, J. Zhao, and R. P. Van Duyne, "Biosensing with plasmonic nanosensors," Nat. Mater. **7**, 442–453 (2008).
2. P. L. Stiles, J. A. Dieringer, N. C. Shah, and R. P. Van Duyne, "Surface-enhanced Raman spectroscopy," Annu. Rev. Anal. Chem. **1**, 601–626 (2008).
3. J. R. Lakowicz, K. Ray, M. Chowdhury, H. Szmacinski, Y. Fu, J. Zhang, and K. Nowaczyk, "Plasmon-controlled fluorescence: a new paradigm in fluorescence spectroscopy," Analyst **133**, 1308–1346 (2008).
4. J. R. Lakowicz, *Principles of Fluorescence Spectroscopy* (Springer, 2006), 3rd ed.
5. P. Schwille and E. Haustein, *Fluorescence Correlation Spectroscopy: An Introduction to Its Concepts and Applications* (Biophysics Textbook Online 1(3), Göttingen, 2001).
6. M. Agio and A. Alú, *Optical Antennas* (Cambridge University, 2013).
7. V. Giannini, A. I. Fernández-Domínguez, S. C. Heck, and S. A. Maier, "Plasmonic nanoantennas: fundamentals and their use in controlling the radiative properties of nanoemitters," Chem. Rev. **111**, 3888–3912 (2011).
8. D. Magde, E. Elson, and W. Webb, "Thermodynamic Fluctuations in a Reacting System - Measurement by Fluorescence Correlation Spectroscopy," Phys. Rev. Lett. **29**, 705–708 (1972).
9. D. Gérard, J. Wenger, N. Bonod, E. Popov, H. Rigneault, F. Mahdavi, S. Blair, J. Dintinger, and T. W. Ebbesen, "Nanoaperture-enhanced fluorescence: Towards higher detection rates with plasmonic metals," Phys. Rev. B **77**, 045413 (2008).
10. J. Wenger, D. Gerard, P. F. Lenne, H. Rigneault, N. Bonod, E. Popov, D. Marguet, C. Nelep, and T. W. Ebbesen, "Biophotonics applications of nanometric apertures," Int. J. Mater. Prod. Tec. **34**, 488–506 (2009).
11. M. J. Levene, J. Korlach, S. W. Turner, M. Foquet, H. G. Craighead, and W. W. Webb, "Zero-mode waveguides for single-molecule analysis at high concentrations," Science **299**, 682–686 (2003).
12. H. Aouani, O. Mahboub, N. Bonod, E. Devaux, E. Popov, H. Rigneault, T. W. Ebbesen, and J. Wenger, "Bright unidirectional fluorescence emission of molecules in a nanoaperture with plasmonic corrugations," Nano Lett. **11**, 637–644 (2011).
13. J. Wenger, H. Rigneault, J. Dintinger, D. Marguet, and P.-F. Lenne, "Single-fluorophore diffusion in a lipid membrane over a subwavelength aperture," J. Biol. Phys. **32**, SN1–4 (2006).

#210904 - $15.00 USD Received 25 Apr 2014; revised 30 May 2014; accepted 30 May 2014; published 17 Jun 2014

14. J. Wenger, D. Gérard, J. Dintinger, O. Mahboub, N. Bonod, E. Popov, T. W. Ebbesen, and H. Rigneault, "Emission and excitation contributions to enhanced single molecule fluorescence by gold nanometric apertures," Opt. Express **16**, 3008 (2008).
15. D. Punj, P. Ghenuche, S. B. Moparthi, J. de Torres, V. Grigoriev, H. Rigneault, and J. Wenger, "Plasmonic antennas and zero-mode waveguides to enhance single molecule fluorescence detection and fluorescence correlation spectroscopy toward physiological concentrations," Wiley Interdiscip. Rev.: Nanomed. Nanobiotechnol. (2014).
16. H. Yuan, S. Khatua, P. Zijlstra, M. Yorulmaz, and M. Orrit, "Thousand-fold enhancement of single-molecule fluorescence near a single gold nanorod," Angew. Chem. Int. Edit. **52**, 1217–1221 (2013).
17. S. Khatua, P. M. R. Paulo, H. Yuan, A. Gupta, P. Zijlstra, and M. Orrit, "Resonant plasmonic enhancement of single-molecule fluorescence by individual gold nanorods," ACS Nano **8**, 4440–4449 (2014).
18. A. Kinkhabwala, Z. Yu, S. Fan, and W. Moerner, "Fluorescence correlation spectroscopy at high concentrations using gold bowtie nanoantennas," Chem. Phys. **406**, 3–8 (2012).
19. L. C. Estrada, P. F. Aramendía, and O. E. Martínez, "10000 times volume reduction for fluorescence correlation spectroscopy using nano-antennas," Opt. Express **16**, 20597–20602 (2008).
20. Q. Wang, G. Lu, L. Hou, T. Zhang, C. Luo, H. Yang, G. Barbillon, F. H. Lei, C. A. Marquette, P. Perriat, O. Tillement, S. Roux, Q. Ouyang, and Q. Gong, "Fluorescence correlation spectroscopy near individual gold nanoparticle," Chem. Phys. Lett. **503**, 256–261 (2011).
21. D. Punj, J. de Torres, H. Rigneault, and J. Wenger, "Gold nanoparticles for enhanced single molecule fluorescence analysis at micromolar concentration," Opt. Express **21**, 27338–27343 (2013).
22. G. Lu, J. Liu, T. Zhang, W. Li, L. Hou, C. Luo, F. Lei, M. Manfait, and Q. Gong, "Plasmonic near-field in the vicinity of a single gold nanoparticle investigated with fluorescence correlation spectroscopy," Nanoscale **4**, 3359–3364 (2012).
23. S. Dutta Choudhury, K. Ray, and J. R. Lakowicz, "Silver Nanostructures for Fluorescence Correlation Spectroscopy: Reduced Volumes and Increased Signal Intensities," J. Phys. Chem. Lett. **3**, 2915–2919 (2012).
24. J. Wenger, "Fluorescence Enhancement Factors on Optical Antennas: Enlarging the Experimental Values without Changing the Antenna Design," Int. J. Opt. **2012**, 1–7 (2012).
25. G. Colas des Francs, A. Bouhelier, E. Finot, J. C. Weeber, A. Dereux, C. Girard, and E. Dujardin, "Fluorescence relaxation in the near-field of a mesoscopic metallic particle: distance dependence and role of plasmon modes," Opt. Express **16**, 17654–17666 (2008).
26. J. Wenger, F. Conchonaud, J. Dintinger, L. Wawrezinieck, T. W. Ebbesen, H. Rigneault, D. Marguet, and P.-F. Lenne, "Diffusion analysis within single nanometric apertures reveals the ultrafine cell membrane organization," Biophys. J. **92**, 913–919 (2007).
27. D. Punj, M. Mivelle, S. B. Moparthi, T. S. van Zanten, H. Rigneault, N. F. van Hulst, M. F. García-Parajó, and J. Wenger, "A plasmonic 'antenna-in-box' platform for enhanced single-molecule analysis at micromolar concentrations," Nat. Nanotechnol. **8**, 512–516 (2013).
28. I. Gregor, D. Patra, and J. Enderlein, "Optical saturation in fluorescence correlation spectroscopy under continuous-wave and pulsed excitation," ChemPhysChem **6**, 164–170 (2005).
29. M. Brinkmeier, K. Dörre, J. Stephan, and M. Eigen, "Two-beam cross-correlation: a method to characterize transport phenomena in micrometer-sized structures," Anal. Chem. **71**, 609–616 (1999).
30. T. Dertinger, V. Pacheco, I. von der Hocht, R. Hartmann, I. Gregor, and J. Enderlein, "Two-focus fluorescence correlation spectroscopy: a new tool for accurate and absolute diffusion measurements," ChemPhysChem **8**, 433–443 (2007).
31. S. T. Hess, S. Huang, A. A. Heikal, and W. W. Webb, "Biological and Chemical Applications of Fluorescence Correlation Spectroscopy: A Review," Biochemistry **41**, 697–705 (2002).
32. G. Mie, "Beiträge zur Optik trüber Medien, speziell kolloidaler Metallösungen," Ann. Phys. **330**, 377–445 (1908).
33. J. Aizpurua, G. W. Bryant, L. J. Richter, and F. J. García de Abajo, "Optical properties of coupled metallic nanorods for field-enhanced spectroscopy," Phys. Rev. B **71**, 235420 (2005).

1. Introduction

One of the promises of plasmonics is the improvement of sensing schemes to the single molecule level. Impressive advances have been made towards this goal utilizing different physical properties, such as refractive index changes [1], Surface enhanced Raman Spectroscopy [2] or fluorescence spectroscopy [3–5]. Especially the detection of fluorescently labeled specimens can profit threefold from properly designed plasmonic antennas: first, the plasmonic antenna can increase the excitation rate by enhancing the local pump-field, secondly, the antenna can funnel the fluorescence emission into a certain direction or polarization state and thirdly, for fluorophores with low intrinsic quantum efficiency the offered additional photonic states of the

#210904 - $15.00 USD Received 25 Apr 2014; revised 30 May 2014; accepted 30 May 2014; published 17 Jun 2014

antenna can greatly improve the quantum yield [6, 7].

Fluorescence correlation spectroscopy [8] (FCS) is widely used to investigate locally the diffusion coefficient of single molecules. FCS exploits random fluorescence intensity fluctuations that occur as individual molecules diffuse into and out of focus in a confocal measurement configuration. These random fluctuations are correlated on a time scale given by the diffusion constant. By its very nature, diffusion measuremens via FCS require the number of detected molecules (fluorophores in the diffraction limited focus) to fluctuate significantly due to brownian motion, which limits the maximal concentration at which FCS measurements can be performed with a standard diffraction limited excitation volume. This limitation can be overcome by employing plasmonic antennas for light and two quintessential geometries have emerged for plasmon enhanced FCS: nano-apertures and nano-antennas. Small nano-apertures in a metal film [9,10], effectively block the background signal by an optically thick metal layer. They have proven to be very useful for FCS measurements [11–14] by shifting the limit of the highest concentration at which measurements are possible by 2-3 orders towards physiologically relevant concentrations [15]. This improvement is mostly due to geometric confinement of the detection volume. Nano-antennas [16,17] also localize fields in deep-sub-wavelength volumes but do not provide an effective suppression of the excitation focus in the solute, which reduces the benefits of the strong field confinement around the antenna in fluorescence fluctuation measurements unless the intensity enhancement at the antenna is very large. Several reports have recently claimed FCS enhancement in plasmon antennas, notably including the bow tie antenna [18] famous for its large field enhancement, as well as simple colloidal metal nanoparticles [19–22] or self assembled silver nano-islands [23].

In this article, we model the effect of nano-antennas, or any other object causing a non-gaussian intensity distribution, on fluorescence fluctuation measurements and identify which configurations actually improve an FCS measurement. In the first section we revisit the established standard FCS theory [4, 5] for Molecular Detection Functions (MDF) of single gaussian shape and recollect the mathematical formalism describing how information is extracted from fluctuating fluorescence intensities and how they are related to the diffusion process in the analyte. Then, we derive expressions which allow to calculate the autocorrelation functions for arbitrary detection volumes and find similarities to expressions derived in dual focus fluorescence cross correlation spectroscopy [29]. In section 3, we apply our model to nano-antenna enhanced FCS experiment by constructing a simplified MDF of only two Gaussian constituent, one representing the diffraction limited '*background focus*', as in standard FCS and additionally we superimpose a second smaller Gaussian '*hotspot*' which represents the confined and enhanced nearfield intensity created by the nano-antenna. Exemplified by this model system, we quantify the benefit for a FCS measurement, that can be obtained depending on intensity enhancements and sizes of the hotspot. We predict the suitability of realistic nano-antennas for improving an FCS measurement by locating their nearfield parameters, extracted from literature, into our parameter phase space diagram. In the last section we discuss in which cases the total correlation function can be used to extract information about the hotspot size and or intensity. Finally we identify in which limits it is valid to interpret a nano-antenna enhanced FCS measurement by a simple single focus FCS model.

2. Fluorescence fluctuation correlation

In a typical Fluorescence Correlation Spectroscopy measurement [8], a collimated laser is focused by a microscope objective in a solution of fluorophores which undergo brownian motion. The fluorescence signal is picked up through the same objective, passes a spectral filter to block the scattered laser light and the fluorescence is then detected on a sensitive detector and stored as a function of time $F(t)$. The temporal fluctuations in the fluorescence intensity originate

#210904 - $15.00 USD Received 25 Apr 2014; revised 30 May 2014; accepted 30 May 2014; published 17 Jun 2014

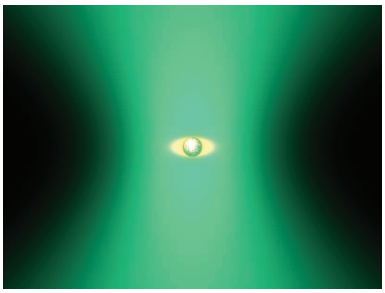

Fig. 1. Schematic of a non-Gaussian MDF: a focused laser beam (green) illuminates a metallic nano-particle (center) which gives rise to field enhancement in its vicinity (orange).

from single molecules randomly entering and leaving the focus. The stochastic trajectories are reflected in temporal correlations in the fluorescence signal. Those correlations are extracted by autocorrelating the fluorescence intensity $G(\tau) = \langle F(t)\, F(t+\tau)\rangle / \left(\langle F(t)\rangle \langle F(t)\rangle\right)$ where the angle brackets denote the average of the signal over time $\langle F(t)\rangle = T^{-1}\int_0^T F(t)\,\mathrm{d}t$. For convenience in notation we define $G'(\tau) = G(\tau) - 1$. The fluorescence intensity $F(t)$ is linked to the spatial distribution of fluorophores $C(\mathbf{r},t)$ by the MDF: $F(t) = B\int \mathrm{MDF}(\mathbf{r})\, C(\mathbf{r},t)\mathrm{d}^3\mathbf{r}$ [4]. The $\mathrm{MDF}(\mathbf{r}) = I_{exc}(\mathbf{r})\,\mathrm{CEF}(\mathbf{r})$ describes the spatial dependence of the detection efficiency of a fluorophore at certain position $\mathbf{r}$ and is defined as the product of the focused excitation beam $I_{exc}(\mathbf{r})$ and the probability to detect fluorescence originating from the same position, quantified by the collection efficiency function $\mathrm{CEF}(\mathbf{r})$. The product of all factors independent from position yields the prefactor B: the excitation power, a setup detection efficiency, the absorption cross-section of the fluorophore and its quantum yield. In an inhomogeneous optical environment (e.g. in the vicinity of a plasmonic antenna) the quantum efficiency is in general also dependent on position [24, 25] and then has to be included as a third factor $\eta(\mathbf{r})$ in the MDF. With this information we can derive a generic expression for the autocorrelation of $F(t)$, given a fluctuating $C(\mathbf{r},t)$

$$G'(\tau) = \frac{B^2 \int \mathrm{MDF}(\mathbf{r}) \int \mathrm{MDF}(\mathbf{r}') \left\langle \delta C(\mathbf{r},0)\, \delta C(\mathbf{r}',\tau)\right\rangle \mathrm{d}^3\mathbf{r}'\mathrm{d}^3\mathbf{r}}{\left[B\langle C\rangle \int \mathrm{MDF}(\mathbf{r})\mathrm{d}^3\mathbf{r}\right]^2}$$

where $\langle \delta C(\mathbf{r},0)\, \delta C(\mathbf{r}',\tau)\rangle$ is the probability to find a fluorophore at time $t+\tau$ on position $\mathbf{r}'$, when it was located at $\mathbf{r}$ at time t. This expression needs a physical model for the motion of the fluorophores in the sample. In the case of free translational diffusion, which we will assume throughout this paper, this term is given by the solution of the diffusion equation $\langle \delta C(\mathbf{r},0)\, \delta C(\mathbf{r}',\tau)\rangle = \langle C\rangle (4\pi D\tau)^{-\frac{3}{2}} \exp\left[-(\mathbf{r}-\mathbf{r}')^2/(4D\tau)\right]$ where D is the diffusion coefficient and $\langle C\rangle$ the average concentration of the fluorophores. Substituting this expression into $G'(\tau)$ yields

$$G'(\tau) = \frac{\int \mathrm{MDF}(\mathbf{r}) \left\{\mathrm{MDF}(\mathbf{r}') * (4\pi D\tau)^{-\frac{3}{2}} \exp\left[-(\mathbf{r}-\mathbf{r}')^2/(4D\tau)\right]\right\} \mathrm{d}^3\mathbf{r}}{\langle C\rangle \left[\int \mathrm{MDF}(\mathbf{r})\mathrm{d}^3\mathbf{r}\right]^2}, \qquad (1)$$

where $*$ denotes convolution. The expression in curly brackets can be intuitively seen as the MDF blurred by the diffusion process with a Gaussian of width $4D\tau$. The volume integrated product of the blurred MDF with the original one quantifies the time evolution of the probability to detect the particle at a time $t+\tau$ again after it has been detected at t.

In standard FCS applications, the MDF is approximated as a single 3D Gaussian determined

#210904 - $15.00 USD Received 25 Apr 2014; revised 30 May 2014; accepted 30 May 2014; published 17 Jun 2014

by its strength S, center position $\mathbf{R}$ and width in each dimension σ

$$\Gamma(\mathbf{r},S,\mathbf{R},\sigma)=\left(\frac{2}{\pi}\right)^{\frac{3}{2}}\frac{S}{\sigma_1\,\sigma_2\,\sigma_3}\exp\left[-2\sum_{k=1,2,3}\left(\frac{r_k-R_k}{\sigma_k}\right)^2\right].$$

This allows an analytical solution of Eq. (1) which then reads [4, 5]

$$G'(\tau)=\left[\langle C\rangle\prod_{k=1,2,3}\sqrt{\pi}\sqrt{4D\,\tau+\sigma_k^2}\right]^{-1}.$$

The correlation contrast is defined as $G'(0)=\left[\langle C\rangle\;\pi^{3/2}\,\sigma_1\,\sigma_2\,\sigma_3\right]^{-1}$. The contrast is the inverse of the average number of fluorophores which contribute to the fluorescence signal $\langle N\rangle$, given the effective detection volume V^* of $\pi^{\frac{3}{2}}\,\sigma_1\,\sigma_2\,\sigma_3$. The peak value is given by the ratio of the volume integral S divided by the effective volume $P=S/V^*$. Assuming a rotation symmetric Gaussian with $\sigma_1=\sigma_2=s$; $\sigma_3=u$ yields the forms of $G(\tau)$, $\langle N\rangle$ and V^* known from FCS literature [4, 5].

2.1. MDF of arbitrary shape

In a nano-antenna enhanced FCS experiment, an antenna is positioned in the focus of a tightly focused laser beam to locally enhance the pump field as well as the detection probability [9–12, 14, 21, 26, 27]. Generally the presence of the antenna results in a MDF that is not simply gaussian. We now introduce a framework to calculate the autocorrelation $G'(\tau)$ for such an MDF. Since a single Gaussian MDF allowed an easy mathematical treatment, we propose to describe any MDF as a sum of Gaussians

$$\mathrm{MDF}(\mathbf{r})=\sum_{i=1}^{N}\Gamma_i(\mathbf{r})=\sum_{i=1}^{N}\Gamma(\mathbf{r},S_i,\mathbf{R}_i,\boldsymbol{\sigma}_\mathbf{i}). \tag{2}$$

It is evident that such a Gaussian expansion can approximate any MDF with arbitrary precision, since in the limit of $\sigma\to 0$ the Gaussians tend to δ-functions, which form a complete set.

In a plasmon enhanced FCS experiment, we would choose the first Gaussian Γ_1 to correspond to the diffraction limited pump spot as in standard FCS. We add the local pump field enhancement of the nano-antenna with one narrower Gaussian Γ_2. More Gaussians can be added to map the pump field distribution more accurately or to account for the suppression of fluorescence emission by quenching in close proximity to the metal surface. Inserting a sum of Gaussians (Eq. (2)) into the general definition of the normalized autocorrelation function (Eq. (1)) yields:

$$G'(\tau)=\frac{1}{\langle C\rangle\,S_{MDF}^2}\left[\Sigma_n A_{n,n}(\tau)+\Sigma_{n\neq m}A_{n,m}(\tau)\right] \tag{3}$$

with $(n,m=1\ldots N)$.

The square brackets consists of N^2 summands, each of them a volume integral of the product of two Gaussians $A_{n,m}(\tau)=\int\Gamma_n(\mathbf{r})\cdot\Gamma_m^D(\mathbf{r},\tau)\,\mathrm{d}^3\mathbf{r}$. As in Eq. (1), the second Gaussian Γ_m is broadened by the convolution with the diffusion kernel. Since the diffusion kernel is also gaussian with a τ-dependent width, the convolution yields again a Gaussian

$$\Gamma_m^D(\mathbf{r},\tau)=\Gamma\left(\mathbf{r},S_m,\mathbf{R}_m,\sigma_m^D(\tau)\right)=\Gamma_m(\mathbf{r})*(4\pi D\tau)^{-\frac{3}{2}}\exp\left[-\left(\mathbf{r}-\mathbf{r}'\right)^2/(4D\,\tau)\right]$$

#210904 - $15.00 USD Received 25 Apr 2014; revised 30 May 2014; accepted 30 May 2014; published 17 Jun 2014

with a τ-dependent width of $\sigma^D_{m,k}(\tau) = \sqrt{{\sigma_{m,k}}^2 + 8D\tau}$. The volume integral $A_{n,m}(\tau)$ is then given by

$$A_{n,m}(\tau) = S_n S_m \prod_{k=1,2,3} \left[\frac{\sqrt{2}}{\sqrt{\pi}\sqrt{\left[\sigma_{n,k}\right]^2 + \left[\sigma^D_{m,k}(\tau)\right]^2}} \exp\left(-2\,\frac{(\mathrm{R_{n,k}} - \mathrm{R_{m,k}})^2}{\left[\sigma_{\mathrm{n,k}}\right]^2 + \left[\sigma^{\mathrm{D}}_{\mathrm{m,k}}(\tau)\right]^2} \right) \right]. \quad (4)$$

The overall normalization factor in Eq. (3) is given, as in the normal single focus FCS, by the square of the volume integral of the entire MDF times the concentration $\langle C\rangle\, S^2_{MDF} = \langle C\rangle \left[\Sigma^N_{n=1} S_n\right]^2 = \langle C\rangle \left[\Sigma^N_{n=1} \int \Gamma_n(\mathbf{r})\, \mathrm{d}^3\mathbf{r}\right]^2$. Equation (4) can be applied to a vast variety of FCS experiments with nontrivial intensity distributions, e.g. standard single focus FCS at intensities where fluorescence saturates in the focus [28], multifocus FCS [29, 30] or FCS experiment with a complex intensity distribution for instance occurring at nano-antennas. The decomposition into Gaussians allows calculating the autocorrelation for any Molecular Detection Function.

We recognize two different types of contributions: $A_{n,n}$ terms correspond to the standard single focus FCS measurements in each Gaussian, whereas the $A_{n,m}$ ($m \neq n$) correspond to contributions of diffusion from one Gaussian to another, as it is established in dual-focus cross correlation FCS experiments [29]. In the case of pure diffusive transport it can be rigorously shown that $A_{n,m}(\tau) = A_{m,n}(\tau)$, thus the number of independent summands reduces to $\frac{1}{2}N(N+1)$. While the ACF obtained from an FCS measurement of *multiple species* in a single focus [4, 31] shows strong similarities to Eq. (3), it lacks the crossterms $A_{n,m(n\neq m)}$. As we will see in Fig. 3(a) in the following section, the crossterm can have a higher contribution to the correlation function than an associated diagonal term. Therefore employing a multi-species model for a multi-gaussian detection experiment as done in [20, 21] to explain the ACF for a plasmonic structure can lead to erroneous results. The cross-terms are well known in dual focus FCS [30], where one creates two spatially separated diffraction limited foci from which autocorrelations $A_{n,n}$ and cross correlations $A_{n,m}$ can be separately measured. For plasmon-antenna enhanced FCS, however, only the sum of all terms can be measured.

3. Two coinciding Gaussians

We now apply our formalism to the case of plasmon enhanced FCS. In particular we consider a scenario where a plasmonic antenna is illuminated by a focused laser beam, as illustrated in Fig. 1. If the excitation wavelength overlaps with an antenna resonance, the electric field intensity $|E_2|^2$ will be locally enhanced close to the antenna compared to the intensity in absence of the antenna $|E_1|^2$.

We show in section 3.2 how the field enhancement contributes to the total correlation contrast. In particular we calculate how one should optimally design the enhancement and volume of a plasmonic hotspot to obtain the highest $G'(\tau = 0)$ at a given concentration, which is of large importance in the quest to apply FCS at physiological concentrations [15]. Afterwards we investigate (section 3.3) how the antenna affects the roll-off time of $G'(\tau)$ for $\tau > 0$. This question is relevant from two distinct viewpoints: on the one hand, given a known solution of fluorophores, one can ask how trustworthy an FCS measurement is to determine the hotspot size and volume. On the other hand, one can ask how suited a given plasmon antenna is to determine the concentration and diffusion constant of a given solute accurately.

In order to answer these questions we consider a very simple model of plasmon-enhanced FCS. For the sake of simplicity we compose the MDF as the superposition of only two coinciding spherical Gaussians ($\mathbf{R_1} = \mathbf{R_2}$; $\sigma_{n,1} = \sigma_{n,2} = \sigma_{n,3}$), one representing a diffraction limited focus Γ_1 and another representing the locally enhanced near-field Γ_2 with smaller extent

#210904 - $15.00 USD Received 25 Apr 2014; revised 30 May 2014; accepted 30 May 2014; published 17 Jun 2014

($\sigma_2 < \sigma_1$). Figure 2(a) shows a typical example of such a scenario. Superimposed in the cen-

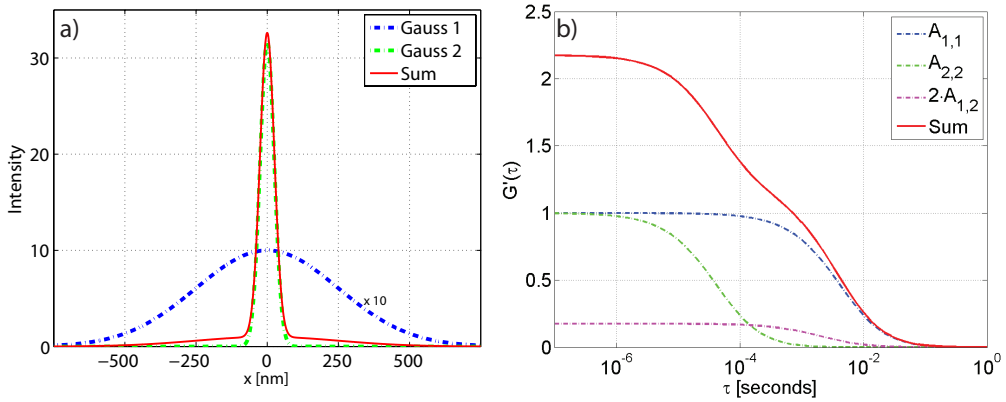

Fig. 2. a) crosscut though a MDF (red line) constructed of two Gaussians: a wide Gaussian (blue dashed line, width: $\sigma_1 = 500$ nm; peak height: $P_1 = 1$; integral: $S_1 = 0.7\mu\text{m}^3$), representing a diffraction limited focus and a narrow Gaussian (green dashed line; $\sigma_2 = 50$nm; $P_2 = 31$; $S_2 = 0.023\mu\text{m}^3$) mimicking a 'hot spot' of a plasmonic nanoparticle. b) Calculated autocorrelation function for the entire MDF (red solid line) and its constituents: the autocorrelation of background focus $A_{1,1}$ (blue dashed line), the hotspot $A_{2,2}$ (green dashed line) and the sum of the identical cross-terms $2A_{1,2}$ (magenta dashed line).

ter of a focus of 500 nm width we consider a hot spot 50 nm across, reaching an intensity enhancement of ≈ 30 in its peak position, a typical value for a metal nano-sphere. By that we assume that the increase of the MDF is only caused by near-field intensity enhancement $P_2/P_1 = |E_2|^2/|E_1|^2$. Quenching could be easily incorporated into the model by including an additional even narrower Gaussian with negative peak height to the sum. Calculations (not shown) with a third Gaussian accounting for quenching have shown negligible influence of the quenching on the total correlation function in a scenario presented in Fig. 2. The calculated $G'(\tau)$ (Fig. 2(b), red solid line) clearly shows an enhanced contrast (the diffraction limited Gaussian only (not shown) would show a contrast of 1) and consists of three contributions: $A_{1,1}$ (blue dashed line) the contribution of the background focus and $A_{2,2}$ (green dashed line) from the hotspot are the main contributions to c, but in addition the contribution of the two identical cross-terms $A_{1,2}$ and $A_{2,1}$ is not negligible (magenta dashed line). Furthermore we see that the influence of the hotspot reduces the roll-off time. The width ratio $\sigma_2/\sigma_1 = 10^{-1}$ translates into a ratio of effective volumes of $V_2^*/V_1^* = 10^{-3}$. The hotspot *alone* would therefore exhibit a correlation contrast $1000\times$ higher than the focus volume, whereas the superposition illustrated in Fig. 2(a) shows a correlation contrast only twice as large as from the bare focus. This shows the importance to properly account for the background focus when conducting an antenna-enhanced FCS measurement.

3.1. Different contributions to the total correlation contrast

We now proceed to find the ideal parameters for the hotspot to enhance the total correlation contrast. Because the total correlation contrast is always inversely proportional to the concentration of the fluorophores, increasing the contrast by utilizing a hotspot allows to measure at higher concentrations. To understand when the correlation contrast is maximum, we extract the relative contributions of the hot spot and the background focus. To compare the relative contributions, we calculate $A_{n,m}$ at $\tau = 0$ for $n = m = 1,2$. With $\mathbf{R_1} = \mathbf{R_2}$ Eq. (4) simplifies to

#210904 - $15.00 USD Received 25 Apr 2014; revised 30 May 2014; accepted 30 May 2014; published 17 Jun 2014

$$A_{n,m}(0) = S_n S_m \prod_{k=1,2,3} \frac{\sqrt{2}}{\sqrt{\pi}\sqrt{\sigma_{n,k}^2 + \sigma_{m,k}^2}}. \tag{5}$$

For summands with $n = m$ the expression further reduces to

$$A_{n,n}(0) = \frac{S_n^2}{\pi^{3/2}\,\sigma_{n,1}\,\sigma_{n,2}\,\sigma_{n,3}} = \frac{S_n^2}{V_n^*}\,. \tag{6}$$

This shows that a hotspot of $10\times$ smaller extent ($1000\times$ smaller volume) than the background focus, contributes as much to the total correlation contrast as the background focus, if the hot spot shows a peak intensity of $\sqrt{1000} \approx 30$ higher than the background focus. This is exactly the case we have illustrated in Fig. 2.

As can be seen in Fig. 3(a) (red curves), the cross terms $A_{1,2}(0)$ (dash-dotted line) clearly exceed the background focus contribution $A_{1,1}(0)$ (dashed line) for $\sigma_2/\sigma_1 > 0.2$, although they remain below the diagonal hot spot contribution $A_{2,2}(0)$ (dotted line). Generally the cross term never exceeds the largest diagonal term, but it can significantly exceed the smaller of the two diagonal contributions. Throughout all figures subsequent to 3(a) we plot the complete G', that is the sum of all contributions.

3.2. Total correlation contrast

While in Fig. 2(b) we calculated $G'(\tau)$ for all time differences, we now analyze the contrast at zero time as a function of the hot spot parameters. Figure 3 shows how the total correlation contrast $G'(\tau = 0)$ depends on the width and peak intensity of the hotspot. All calculations shown in this article were performed with a background focus of $\sigma_1 = 500\,\text{nm}$ width, a peak height of $P_1 = 1$ and a diffusion coefficient $D = 10^{-11}\ \text{m}^2\text{s}^{-1}$.

Figure 3(a) displays the total correlation contrast (solid lines) for hot spots with three different peak intensities $P_2 = 1$, 10 and 32 in dependency of the relative width σ_2/σ_1. As expected, the higher the field enhancement, the higher the contrast boost that can be achieved. For a hotspot with ten-fold peak enhancement (solid green line) we see that the total correlation contrast can be increased from 1 to 4 when the hotspot is a third of the size of the diffraction limited spot ($\sigma_2 = 150$ nm). For a peak enhancement of 32 (solid red curve) the correlation contrast can exceed 9 for a hotspot width of $\sigma_2 = 100$ nm ($\sigma_2/\sigma_1 = 1/5$). Maybe more surprisingly, we find that there is an optimum size at which the highest correlation contrast is achieved. This optimum shifts with increasing enhancement factors to smaller hotspot sizes. If a hotspot is too small its contribution to the total fluorescence signal is too small to influence $G'(\tau)$. If on the other hand the hotspot is too big (about the size of the focus field), there is no reduction in effective volume, thus no increased correlation contrast.

Figure 3(b) provides an overview of $G'(0)$ in a larger parameter space in a color plot with logarithmic color scale and the width ratio σ_2/σ_1 on the horizontal and the peak ratio P_2/P_1 on the vertical axis. We now explore the content of this phase diagram by means of a few limiting cases. At the right side of the diagram at $\sigma_2/\sigma_1 = 1$, the hotspot has the same width as the Gaussian, which is equivalent to just increasing the amplitude of the MDF but leaving its shape unaltered. The ACF is not affected by scaling of the MDF, thus $G'(0) = 1$, independent of P_2/P_1. In other words, there is no point offering any field enhancement, unless it is confined to a fraction of the focus. A horizontal cut at $P_2/P_1 = 1$ (blue line) corresponds to a hotspot with the same amplitude as the big Gaussian. Walking on a line from right to left corresponds to reducing the size of this hotspot, keeping its amplitude constant at 1. As can be seen in Fig. 3(a) (blue solid line) this improves the total contrast merely from 1 to ≈ 1.3 at $\sigma_2/\sigma_1 \approx 0.6$. Reducing σ_2/σ_1 further makes the contribution of the hotspot vanish: while offering the desired

#210904 - $15.00 USD Received 25 Apr 2014; revised 30 May 2014; accepted 30 May 2014; published 17 Jun 2014

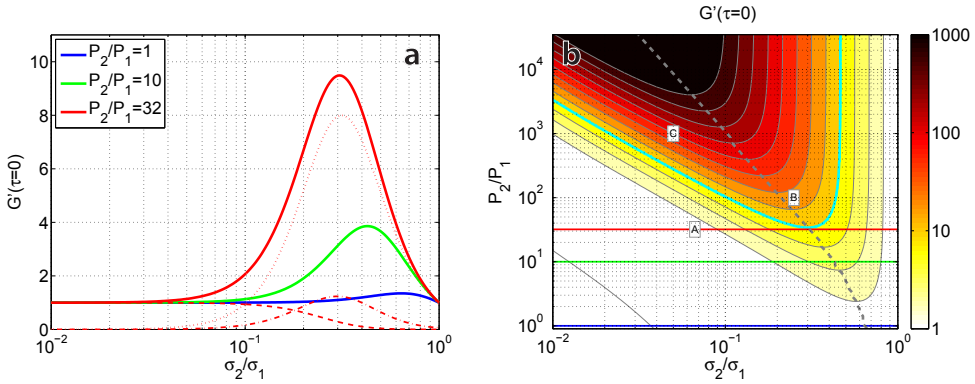

Fig. 3. The background focus is kept constant at $\sigma_1 = 500$ nm and $P_1 = 1$ whereas the parameters of the hotspot are varied. a) The total correlation contrast $G'(0)$ (solid lines) for three different peak to peak ratios. For the red curve ($P_2/P_1 = 32$) we additionally show its constituents: $A_{1,1}$ (dashed line), $A_{2,2}$ (dotted line) and $2A_{1,2}$ (dash-dotted line). In the range of ideal correlation contrast enhancement for a given peak intensity enhancement, the cross term $A_{1,2}$ can have a stronger influence on the total correlation function than the background focus $A_{1,1}$ itself. The time dependence of the red curves at $\sigma_2/\sigma_1 = 10^{-1}$ is shown in Fig. 2(b).
b) Shows how the total correlation contrast depends on the relative width σ_2/σ_1 and relative peak intensities P_2/P_1. The cyan line indicates where the total correlation contrast is $10\times$ enhanced compared to the bare background focus. Crosscuts along the blue, green and red lines corresponds to the solids lines in Fig. 3 of the same colors. The gray dashed line shows which relative width yields the maximum contrast for given peak intensities. The labels A,B,C denote realistic antenna parameters from literature listed in Table 1.

confinement -which is a prerequisite for high FCS contrast- the fewer molecules in the hot spot generate strong relative fluctuations in the hotspot fluorescence but they simply provide insufficient photon counts compared to those in the background focus. If we now consider a vertical cross section at $\sigma_2/\sigma_1 = 10^{-1}$, increasing the field intensity enhancement, at first the contrast barely increases. When crossing the horizontal red line at $P_2/P_1 = 32$ the contrast has doubled to $G'(0) \approx 2$, meaning that the hotspot has gained enough intensity to contribute the same amplitude to the total correlation function as the background focus (as in Fig. 2). Increasing the peak height of the hotspot further greatly improves the total correlation contrast until it saturates at $P_2/P_1 \approx 10^4$ approaching $G'(0) \approx 1000$ associated with the 1000 times smaller volume of the hotspot. For higher enhancements the $G'(\tau)$ is fully determined by the signal from the hotspot and the background focus is not relevant anymore.

We notice that on horizontal cross sections, at any given peak enhancement, there is an optimal size of hotspot to maximally increase the total correlation contrast, exactly as seen in the cross cuts in Fig. 3(a). The gray dashed line in Fig. 3(b) indicates the optimum hotspot size for each enhancement. The optimum shifts to smaller hot spot sizes for larger enhancements. Having mapped the influence on the total correlation contrast of certain hotspots for FCS, we wonder where actual plasmonic antennas reside in this diagram. Indeed, fluorescence fluctuation measurements have recently been reported for Au-spheres, bow-ties antennas and nano-rods [16, 18, 21]. For the bow-tie and nano-rod antennas we have estimated the field enhancement and their extents from literature calculations. For gold nano-spheres we have calculated field enhancements and extents using analytical Mie theory [32]. The hotspot parameters extracted or calculated for three realistic antennas we have compiled in Table 1. The labels *A*, *B*

#210904 - $15.00 USD Received 25 Apr 2014; revised 30 May 2014; accepted 30 May 2014; published 17 Jun 2014

Table 1. Properties of gold nano-antennas in literature: A) Gold Mie sphere (∅100 nm); near field intensity enhancement was calculated and σ_2 was approximated by the cubic root of the calculated effective mode volume; B) single nanorod ([33], Fig. 2(b) inset), hotspot diameter approximated by rod diameter; C) Bow tie antenna [18], hotspot diameter approximated by the gap size. All hotspot diameters were put into ratio to the extend of the background focus given by a diffraction limited focus of $\sigma_1 = \lambda/(2\,\mathrm{NA})$ assuming a NA=1 objective.

	Structure	σ_2	$(E_2/E_1)^2$	λ_0	$\sigma_1 = \lambda_0/2$	σ_2/σ_1
A	Au sphere	20 nm	32	580 nm	290 nm	1/15
B	single nanorod	80 nm	100	620 nm	310 nm	1/4
C	Bow Tie antenna	20 nm	1000	780 nm	390 nm	1/20

and *C* in Fig. 3(b) show where these antennas reside in our hotspot parameter space. Evidently Mie spheres (label *A*) supply poor intensity enhancement and are too confined to yield optimal FCS enhancement. This is compatible with the experimental findings of a total correlation contrast enhancement of $\approx 2\times$ and $\approx 12\times$ for gold colloids in [20] and [21], taking into account the different quantum efficiencies used in the experiments.

Estrada et al. have shown measurable correlation contrast assisted by a gold colloid (∅80 nm) in a 150μM dye-solution, '10^4 times the concentration used in standard experiments' [19]. The reported experiment could not pinpoint the origin of the enhanced correlation, and an equal contribution of altered molecule kinetics by sticking at interfaces and reduced diffusion volume is suggested by the authors. Our model suggests that the reduced volume for freely diffusing particles is unlikely to have such a strong effect in the described system.

Nano-rods (label *B*) perform much better due to their higher intensity enhancement. The bow tie antenna (label *C*) seems ideal and our model predicts a 1000-fold increase in correlation contrast might be reached. It should be noted that in the experimental realizations of the latter two antennas [16, 18], the fluorescence fluctuations signal was afflicted by 'sticking' dynamics of the fluorophores to the particle or substrate surface, thus those experimental correlation functions can not be compared with our model which only includes diffusion. A recent experiment by Punj et al. [27] has quantified the correlation enhancement for a so called 'antenna in a box', a particle dimer antenna enclosed in a rectangular void in a gold film. They established detection volumes down to 60 zl, meaning a factor 30 contrast enhancement compared to a reference measurement that utilized the same rectangular void but without bow tie. This reference measurement in itself already implied a 100-fold reduced detection volume compared to a free focus.

3.3. τ dependence of $G'(\tau)$

The correlation contrast at zero time is important because it directly determines the maximal concentration at which fluctuations measurements can be performed. However measuring a diffusion constant requires the measurement of the roll off time of $G'(\tau)$. On the one hand one can ask how suited a given plasmon antenna is to determine the concentration and diffusion constant of a given solute accurately. On the other hand, given a known solution, it is interesting to check how trustworthy an FCS measurement is to determine the hot spot volume from a measured diffusion time. We define the effective diffusion time τ^* as the time when $G'(\tau)$ has dropped to half its maximum value $G'(\tau^*)/G'(0) = 1/2$. Figure 4(a) shows the effective diffusion time as a function of the hot spot parameters.

We explore the meaning of Fig. 4 by again walking along limiting cases. The different limits in this diagram are as follows: When the hotspot is the size of the background focus

#210904 - $15.00 USD Received 25 Apr 2014; revised 30 May 2014; accepted 30 May 2014; published 17 Jun 2014

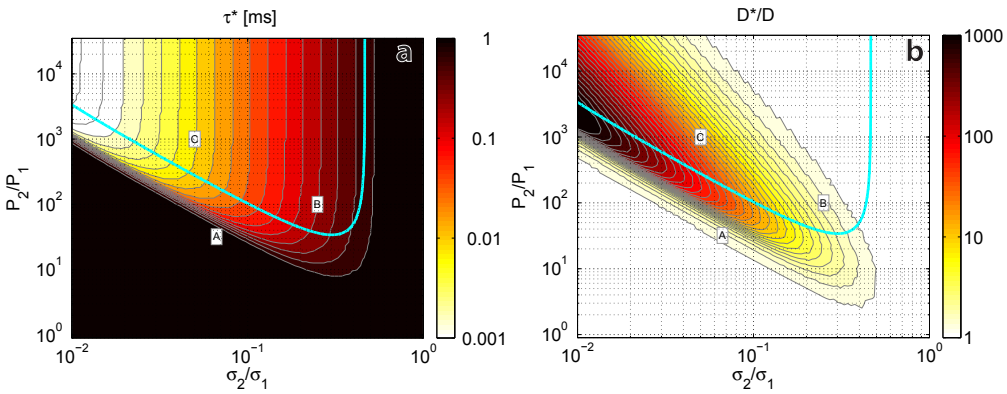

Fig. 4. a) Shows how the effective diffusion time τ^* of the total correlation function depends on the hotspot size and amplitude. The apparent diffusion coefficient D^* was extracted from $G'(0)$, τ^* and known concentration assuming a single focus FCS experiment. b) Shows the ratio D^*/D_0 of the apparent divided by the real diffusion coefficient, showing a possible misjudging of $1000\times$ in the calculated parameter range. The cyan lines (from Fig. 3(b)) shows the parameters for which the total correlation contrast in enhanced $10\times$.

($\sigma_2/\sigma_1 = 1$), the diffusion time is unaffected because the shape of the MDF is unchanged. When the enhancement is very low (e.g. $P_2/P_1 = 1$), the diffusion time is dominated by the background focus and shrinking the hotspot further does not change τ^*. Whenever the enhancement is high (e.g. $P_2/P_1 = 10^4$), the total correlation function $G'(\tau)$ is dominated by the hotspot and τ^* then scales like $\propto (\sigma_2)^2$. Now assume we increase the hotspot intensity for a given size (e.g. $\sigma_2/\sigma_1 = 0.1$) starting from $P_2/P_1 = 1$: for a weak hot spot the diffusion time is determined by the background focus but increasing hotspot intensities to ≈ 30 we see a steep transition for τ^* at the point when hotspot and background focus contribute equally to the $G'(\tau)$ (close to label *A*). When we further increase the hotspot intensity the τ^* saturates at the diffusion time of the bare hot spot.

3.4. Retrieval of the information about the hotspot

Having explored how the parameters $G'(0)$ and τ^*, which characterize $G'(\tau)$, behave for different hotspots, we now investigate in which cases we can safely deduce information about the hotspot from the total correlation function $G'(\tau)$. Because fitting a closed expression of $G(\tau)$ for a given number of Gaussian to experimental data is expected to be error-prone, we now attempt to retrieve information from parameters which can be extracted robustly: first, the total correlation contrast $G(0)$ and second the effective diffusion time τ^*.

We assume to have a calibrated solution of known diffusion coefficient and concentration which could for instance be measured via a standard single focus FCS measurement in the same solution without the antenna. Performing a measurement on the antenna yields a different correlation contrast $G'(0)$ and diffusion time τ^*. If the concentration is known, the correlation contrast $G'(0)$ allows to retrieve the effective volume V^*. If the correlation contrast is more than $10\times$ enhanced (above the cyan contour line in Fig. 3(b) and Fig. 4(a,b) the measured diffusion time τ^* is in good approximation determined by the hotspot. This can be seen in Fig. 4(a) as τ^* does not change with changing field enhancement anymore. Thus in this case one can deduce the extent σ_2 of the hotspot by the measured diffusion time and the known diffusion coefficient D, and neglecting the background focus. Having determined σ_2 from the effective diffusion time one has essentially fixed the position on the horizontal axis in our color plots. If the boost

#210904 - $15.00 USD Received 25 Apr 2014; revised 30 May 2014; accepted 30 May 2014; published 17 Jun 2014

in correlation contrast is not at the limit of the bare hotspot of $(\sigma_2/\sigma_1)^{-3}$, meaning the contour lines in Fig. 3(b) are *not* vertical yet, then this value of $G'(0)$ corresponds to an unique peak enhancement P_2/P_1 for the antenna. In other words, a FCS measurement at an antenna in a calibrated solution allows to retrieve the size and the peak enhancement of the hotspot just by extracting $G'(0)$ and τ^*, if the temporal shape of $G'(\tau)$ is dominated by the hot spot.

3.5. Retrieval of the Diffusion coefficient

We just have examined in which cases the total correlation function allows reading off hot spot properties. Now we ask in which conditions the antenna enhanced FCS can be used to measure the diffusion coefficient of an unknown solution. If the very same antenna was calibrated in reference measurement (with known diffusion coefficient D_0 and concentration C_0) the measurement of the unknown solution can be compared to the reference and hence the diffusion time and total contrast can be related to the diffusion constant and concentration of the reference. It should be noted, that due to the dispersive character of a plasmonic antenna the calibration has to be carried out within the same dielectric environment (refractive index of the solvent) with a fluorophore showing the same absorption and emission spectrum as well as the same quantum efficiency as the target solution. Moreover we expect that one should use exactly the same antenna as field enhancements may vary strongly between nominally identical antennas.

If a full calibration of the nano-antenna is not possible but either the diffusion constant or the concentration of the solution is known, one might be tempted to extract too much information from $G'(\tau)$. As an example we assume that the average concentration C_0 is known and calculate the diffusion coefficient from $G'(0)$ and τ^*. From the total correlation contrast $G'(0)$ and a known concentration C_0 we calculate the effective volume $V_{eff} = (G'(0)\,C_0)^{-1}$ and assume spherical symmetry to get the effective width of the Gaussian $\sigma_{eff} = \pi^{-1/2}\,V_{eff}^{1/3}$. Next we take the effective diffusion time τ^* to then calculate the theoretical diffusion constant $D^* = (\sigma^*)^2/(4\,\tau^*)$. Figure 4(b) shows the ratio D^*/D_0 of the calculated diffusion coefficient divided by the real diffusion constant used in the calculations. We see that the diffusion coefficient maybe misjudged by a factor of 1000 when interpreting the correlation curve as in a single focus FCS experiment. Only in two limits does this retrieval yield a correct diffusion coefficient. These two cases are on the one hand, when the hot spot does not affect the $G'(\tau)$ at all, namely at low peak enhancements, or on the other hand at very high peak enhancements when the hotspots totally dominate $G'(\tau)$, which is the case at regions where the contour lines in Fig. 3(b) *and* Fig. 4(a) are vertical. Unfortunately, especially the regions in parameter space of realistic plasmonic antennas yields diffusion coefficients up to a factor 100 higher than the real value.

4. Conclusion

We have presented a mathematical framework to treat fluorescence correlation measurements of systems with a non-gaussian Molecular Detection Function, as in the case of nano-antenna enhanced FCS measurement. In a plasmonic environment the MDF is the product of the pump field intensity, the detection efficiency and the quantum efficiency, where all quantities are dependent on position and require the spatial mapping of electromagnetic field at the excitation wavelength, at the emission wavelength and the local density of optical states at the emission frequency. Once obtained, the MDF can be decomposed into Gaussians and the expressions we derived allow an analytical treatment of simple problems or efficient numerical handling for MDFs of arbitrary complexity.

For the example of a plasmon enhanced FCS experiment approximated by two Gaussians, mimicking the diffraction limited background focus and the nano-antenna hotspot, we dis-

#210904 - $15.00 USD Received 25 Apr 2014; revised 30 May 2014; accepted 30 May 2014; published 17 Jun 2014

cussed how the hotspot affects the total correlation function. Marking realistic values for plasmonic hotspot sizes and peak amplitudes in our calculations allows the prediction of their benefit for FCS applications. We found that a bow tie antenna can outperform a Mie sphere by two orders of magnitude in terms of increasing the total correlation contrast, due to its field enhancement being $30\times$ higher than the Mie sphere. Further we showed that for a given hotspot peak intensity, there is an optimal size at which the total correlation contrast becomes maximal. Characteristic parameters of the correlation function like total contrast and diffusion time scale differently with the hotspot width or peak height. This has severe implications: even if the total correlation function seems to be dominated by the hotspot –exhibiting strongly increased contrast or significant reduction of the diffusion time– this does in general not allow to interpret the total correlation function as in a single focus FCS experiment and leads to diffusion coefficients orders of magnitudes different from the real value. We identify hotspot parameter regimes in which an interpretation of the correlation curve as in a single focus experiment is tolerable and yields correct results. Our model is a versatile tool to efficiently predict how non-gaussian intensity distributions alter fluorescence fluctuation measurements. As such it allows to benchmark proposed antenna designs for FCS against the requirements that MDF enhancements of at least around 10^2 are obtained and that the antenna sustains such a high MDF over a sufficiently large volume to maximally improve FCS contrast. This is by no means an easy challenge, as large MDF enhancements typically involve narrow gaps.

Acknowledgments

We are grateful to Clara Osorio and Artem Bakulin for carefully reviewing the manuscript. This work is part of the research program of the Foundation for Fundamental Research on Matter (FOM), which is financially supported by the The Netherlands Organization for Scientific Research (NWO). This work is supported by NanoNextNL, a micro- and nanotechnology consortium of the Government of The Netherlands and 130 partners. A.F.K. gratefully acknowledges an NWO-Vidi grant for financial support.

#210904 - $15.00 USD Received 25 Apr 2014; revised 30 May 2014; accepted 30 May 2014; published 17 Jun 2014